Solid State Ionics 52 (1992) 57–68
North-Holland

SOLID
STATE
IONICS

Materials considerations for application to solid-state electrochemical devices

A. Khandkar, S. Elangovan and M. Liu
Ceramatec, Inc., 2425 S 900 W, Salt Lake City, UT 84119, USA

An overview of some recent materials-related investigations, aimed at providing a better understanding of their role in enhancement of the performance of high-temperature solid-state electrochemical devices, is given with special reference to solid oxide fuel cells. The limitations of traditional approaches taken to optimize device performance are pointed out and the need to study interactions between materials is emphasized. These considerations arise due to enhanced kinetics at high temperature of interdiffusion and bulk diffusion at solid/solid interfaces which lead to chemical and physical changes at the electrode interfaces. The effect of these changes on device performance and stability are discussed. Relationships between composition–property and processing–microstructure are also discussed. An impedance model, based upon detailed interface investigations is presented.

1. Introduction

Typical high-temperature devices can be classified into two broad categories, (a) potentiometric devices such as sensors which operate on the Nernst principle and yield an EMF corresponding to the measured electrochemical potential of a species against a reference and (b) amperometric devices such as solid oxide fuel cells, electrolyzers and oxygen pumps where a current is drawn/passed proportional to the gradient in electrochemical potential of the electroactive species. Ceramic conducting materials form the basis of these new and rapidly emerging technologies. While devices such as oxygen sensors have already established important technological impact, oxygen concentration devices (or oxygen pumps) and solid oxide fuel cells are in the developmental stage. With the increasing awareness of environmental problems, the science and technology of these devices is being studied with renewed interest. The principal problems with such technologies stem from the high operating temperatures, 800–1000°C, necessary for achieving acceptable ion transport rates as required for practical device applications.

The advantages of high-temperature operation include low electrode overpotential losses and low ohmic losses. While electrode kinetic overpotentials (also termed irreversibility) are inherent in all electrode processes conducted at finite rates, for high-temperature devices additional sources of "irreversibility" exist due to materials interactions. For example, the electrode and interface morphology and phase assemblage undergo a continuous change at high temperatures, leading to the formation of thermodynamically favored resistive layers or physical isolation (as in the case of non-wetting metal on ceramic electrodes, discussed later). These materials-related irreversibilities often limit the performance of high-temperature devices by increasing the cell impedance. Deleterious reactions at electrode–electrolyte interfaces limit performance characteristics due to changes in electrode morphology or interdiffusion of species exacerbated by the high temperatures. Such changes lead to increased overpotentials and are thus termed irreversibilities, otherwise often known as degradation. It is of interest to determine the underlying causes of such degradation in order to improve these characteristics. Detailed understanding of each of the consequent polarization mechanisms thus becomes very critical.

1.1. Characteristics of high performance

High performance in a solid-state electrochemical device may be defined in different ways: in oxygen pumps and fuel cells high performance is achieved when the overall internal resistance of the device is lowered so that large currents can be passed or drawn at low overpotentials. In sensors, high performance may be defined as the speed of response with which the electric signal changes for a given change in concentration of the species being measured. Thus, the following considerations become important for high-temperature systems:

(1) optimization of power density and endurance, requiring materials with stable morphologies and resistance to reactions at interfaces, thus allowing good current densities to be maintained with minimum "losses";

(2) satisfactory thermal cycle life, (at least 40000 h are desired with about 100 thermal cycles), requiring thermo-mechanical stability at interfaces.

The general approach to increasing device performance is often to reduce the thickness of the cells, thus reducing the ohmic resistance contributions and to increase the electrocatalytic activity of the electrodes as in the case of sensors. An alternative approach would be to alter the intrinsic properties of the materials of cell construction such as substituting stabilized zirconia with ceria or bismuth-oxide-based materials for electrolytes.

However, as device geometries become thinner, materials-related degradation effects play a more dominant role in determination of performance. Scanning micrography and X-ray diffraction have been used to identify the principal sources of materials "irreversibility" arising out of reactions at high temperature [1,2]. Recent work on understanding such degradation processes, using impedance spectroscopy (EIS) complemented with traditional methods, has been carried out by the authors in greater detail with reference to SOFCs [3,4]. The SOFC may be considered an ideal cell for the study of materials irreversibilities, which result in cell degradation, due to the possibility of several different types of degradation processes occurring simultaneously.

The EIS technique was used to examine the causes of materials polarization and separate materials irreversibilities from electrode kinetic irreversibility. The technique allows unambiguous separation of these effects only in cases where the characteristic frequencies of the relaxation processes are well separated from each other. The solid oxide fuel cell, comprising of a Ni/ZrO_2 cermet anode, yttria-stabilized zirconia electrolyte and $La(Sr)MnO_3$ ceramic cathode, was used as a case study to illustrate the materials irreversibility since this electrode-electrolyte system provides a most comprehensive overview of the problems. The technique allowed the study of cell-degradation processes under operating conditions. The technique has also been applied to the evaluation of the contributions of electrodes to cell performance degradation in an SOFC subjected to thermal cycling. The analysis was conducted using a planar SOFC cell with reference electrodes which allowed the unambiguous separation of the electrolyte, electrode and interface effects. Based on prior interface degradation studies carried out by these authors [5,6], detailed lumped parameter impedance circuit model of a typical high-temperature cell is derived, similar to that for sodium–sulfur cells [7]. The effect of various polarizations on the impedance spectra are shown for various cases.

1.2. Degradation in sensors and fuel cells

Both solid oxide fuel cells and typical oxygen sensors are comprised of stabilized zirconia as the electrolyte with metal cermet electrodes or perovskite electrodes. Schematic illustrations of these devices are shown in fig. 1. During long-term operation of such devices, the device performance deteriorates which can manifest itself in different ways. For example, in sensors an increase in response time is generally seen due to reduction in charge transfer kinetics [8]; an increase in cell voltage at constant current density is obtained for an oxygen pump and

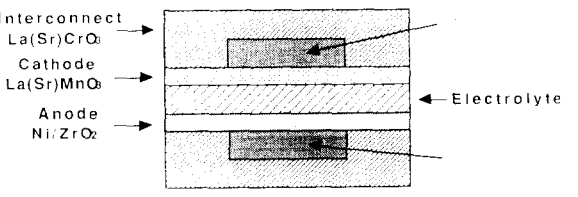

Fig. 1. Schematic of a planar SOFC stack and repeat element.

a reduction in current density at constant applied potential respectively is observed in SOFCs. Fig. 2 shows the I/V characteristics with time for a fuel cell and oxygen pump where in both cases a steady decrease in performance is observed.

1.3. Sources of polarization in a solid oxide fuel cell (SOFC)

To better understand the sources of polarizations, a description of the cell and interfacial reactions is helpful. The overall reactions for an SOFC operating on H_2 and air are associated with the formation of O^{2-} ions at the cathode–electrolyte interface which are transported across the zirconia electrolyte to the anode interface. The ions cross the anode–electrolyte interface and, ideally, are transported through the zirconia cermet in the cermet. Thus the half-cell reactions are:

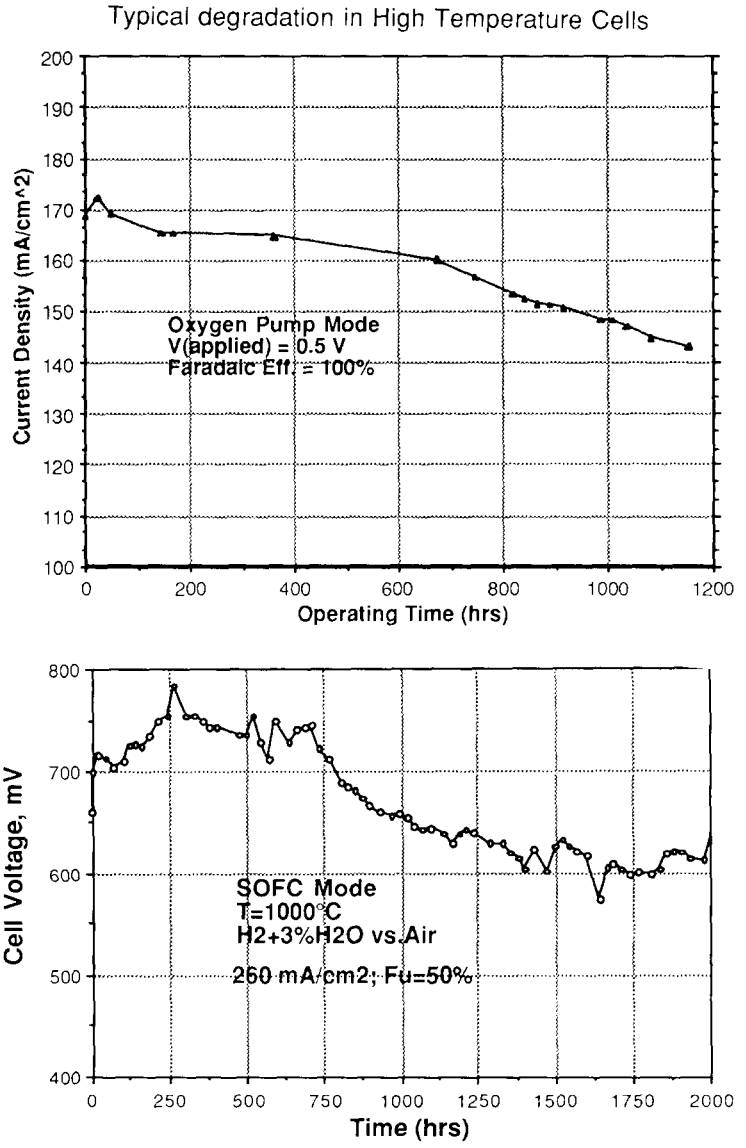

Fig. 2. Typical degradation in high-temperature cells.

$\frac{1}{2}O_2 + 2e^- \Rightarrow O^{2-}$ at the cathode (1)

and

$H_2 + O^{2-} \Rightarrow H_2O + 2e^-$ at the anode. (2)

The description of the cells for oxygen pump and sensors are simpler and, in the former case, consists of a symmetric cell with two noble metal cermets (e.g. Pt/ZrO_2) separated by the electrolyte or, in the latter case, two ceramic electrodes (such as $La(Sr)MnO_3$) separated by the electrolyte.

With reference to the SOFC case, there arise several sources of polarization due to the following:

(1) charge transfer resistance ($\frac{1}{2}O_2/O^{2-}$) at the LSM/ZrO_2 interface;

(2) interfacial blocking effects at the LSM/ZrO_2 interface arising due to the reactivity of LSM with ZrO_2, resulting in the formation of insulating phases such as $La_2Zr_2O_7$;

(3) ionic resistance in the electrolyte;

(4) interfacial effects at the $Ni–ZrO_2/ZrO_2$ interface arising out of time- and temperature-dependent changes at the three-phase Ni/ZrO_2/gas boundary;

(5) charge transfer reaction due to oxidation of H_2; and

(6) contact resistances such as those associated with interdiffusion of isomorphous materials which, in practice, arise in multicell stacks.

The charge transfer resistances are electrode-kinetic-related impedances and their treatment is provided elsewhere [8]. Only the materials-related polarization mechanisms will be considered below. The experimental procedures, results and discussion of the mechanisms are summarized below. Details are given in the pertinent literature.

In the case of SOFCs, the candidate materials used along with stabilized zirconia electrolyte are $La(Sr)MnO_3$ as the cathode and $La(Sr)CrO_3$ as the interconnection. The cathode and the interconnection materials being isostructural lend themselves to interdiffusion of chromium and manganese. Chromium substitution into $La(Sr)MnO_3$ has been shown to decrease its conductivity [9]. In addition, formation of the zirconates of lanthanum and strontium has been reported in a powder mixture of the electrolyte and cathode materials reacted at high temperatures [15]. The effect of these reactions, which leads to changes in "interfacial resistance", on the cell response is measured. Finally, the effect of thermal cycling and the resultant degradation is determined.

2. Experimental

2.1. Interdiffusion at cell interfaces

Air-sintered, fully densified samples of $La(Sr)CrO_3$ (LSC) and $La(Sr)MnO_3$ (LSM) were prepared from liquid mix synthesized powders. Pellets of commercially available coprecipitated (8 mol% Y_2O_3) ZrO_2 (YSZ) were also prepared. Archimedian measurements were made to ensure that all specimens had densities in excess of 95% and open porosities below 0.05%. XRD analysis showed that no impurity phases were present. One face of each sample was polished and optically examined to ensure a clean, flat contamination-free surface. Diffusion couples consisting of electrolyte/cathode and cathode/interconnect pellets were made by placing polished surfaces of the samples in intimate contact and burying them in powders composed of a 50:50 mixture of the component materials in a high-purity alumina crucible. The diffusion couples were annealed at temperatures between 1200°C and 1650°C for periods of 24, 96 and 168 h. The furnace temperature was monitored using a B-type thermocouple and maintained at a constant temperature within ± 5°C for the duration of the run. The annealed samples were quenched in air to room temperature, mounted in an epoxy resin and polished to remove the surface layers to expose the diffusion region. The samples were examined using an electron microprobe. Determination of the compositional profile, perpendicular to the original weld, was achieved by observing the X-ray counts of Cr-K_α, Mn-K_α, Sr-L_β and La-L_α.

2.2. Study of the cathode–electrolyte interface

The cathode material, $La_{0.89}Sr_{0.1}MnO_3$ (LSM), was synthesized using the Peccini process. The calcined powder was characterized to be single-phase using XRD. Tape-cast-stabilized zirconia was used as the electrolyte. The cathode was applied to the electrolyte by the screen-printing process. The elec-

trodes were sintered at various temperatures and times. A fuel cell, with LSM cathode and Ni/ZrO_2 cermet anode, was chosen for the long-term test. The fabrication conditions of the cell were chosen such that the SEM analysis of a representative pre-test cell did not show any evidence of interface reaction product. The fuel cell was run for 1300 h, under load. The cell load was periodically interrupted and the cathode/electrolyte interfacial impedance was measured using Solartron 1286 ECI and Solartron 1250 FRA. In addition, half-cell measurements were performed to compare the interfacial contributions for various fabrication conditions.

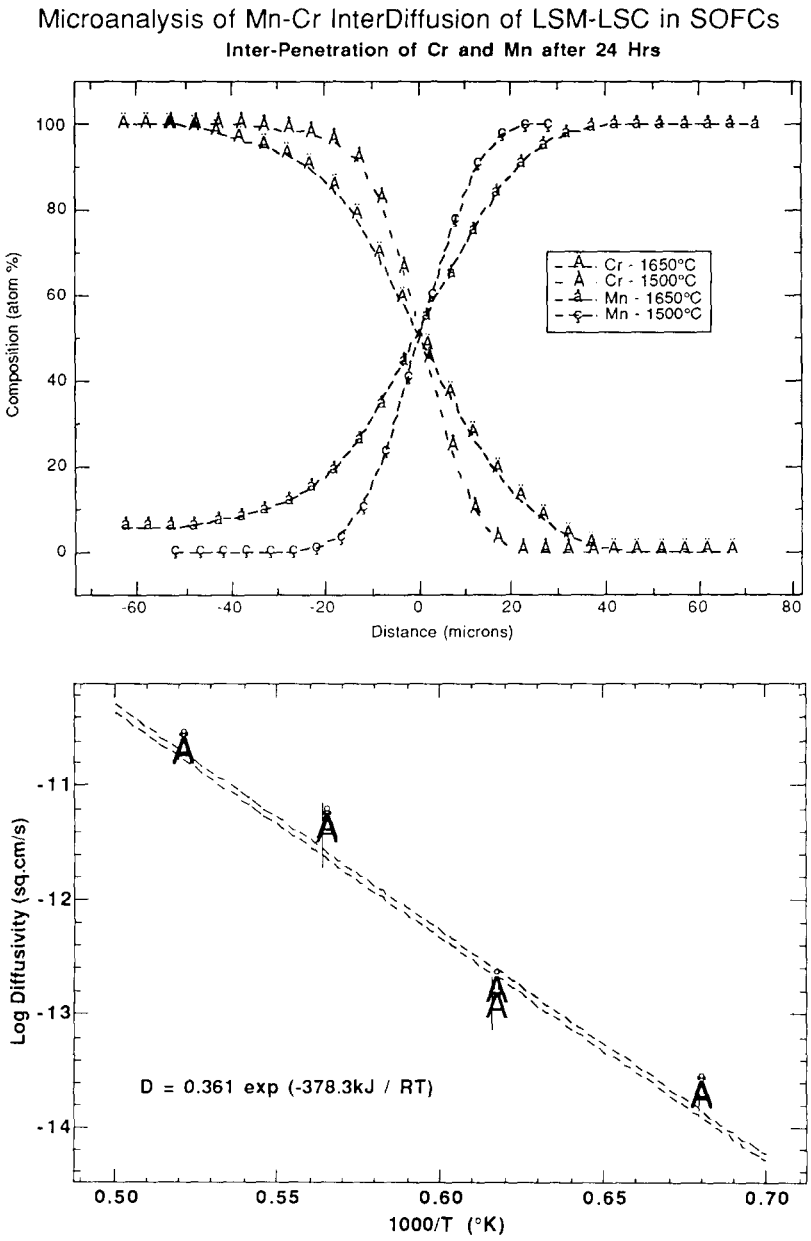

Fig. 3. Microanalysis of Mn–Cr interdiffusion of LSM–LSC in SOFCs.

2.3. Study of thermal cycle related cell degradation

Planar SOFCs using an yttria-stabilized zirconia electrolyte (150 μm thick × 32 mm dia.) with screen-printed electrodes ($La(Sr)MnO_3$ for the cathode and $NiO-ZrO_2$ cermet for the anode, active electrode area ≈ 4.5 cm^2) were fabricated using standard fabrication procedures described elsewhere [3]. The cell configuration included a reference electrode. The electrodes were contacted with a platinum grid using platinum paste (Heraeus) and sealed to a ceramic tube to form the anode and cathode reactant compartments. The cells were operated with H_2–3%H_2O versus air. A cell was initially operated at 1273 K in order to determine the electrode response characteristics and was held under a constant load corresponding to a modest current density of ≈ 100 mA cm^{-2}. After ensuring stable performance for 200 h the cell was thermally cycled to 298 K and heated up at a constant rate. Thermal cycle conditions were varied with respect to cooling rates, loads (i.e. under load or at open circuit) as well as fuel gas atmospheres (i.e. in fuel gas or in air). Impedance spectra were obtained using a Solartron 1255 FRA coupled to a Solartron 1286 ECI. The impedance data, acquired over 7 decades of frequency, were stored in a PC and analyzed using EquivalentCircuit [#1]. Using the appropriate reference electrodes and counter/working electrodes, impedance data were obtained for the cell including the electrodes, the electrolyte and the platinum current collector grid and the anode and cathode interfaces separately.

[#1] B. Boukamp, University of Twente, The Netherlands.

3. Results and discussion

3.1. Interdiffusion of chromium and manganese across LSM–LSC interfaces

The composition profiles of manganese and chromium, in the $La(Sr)MnO_3$–$La(Sr)CrO_3$ system, at two temperatures (1500 and 1650°C) after 24 h of annealing are shown in fig. 3a. The composition profile was analyzed using the Matano method [10] as well as the error function method to determine the interdiffusion coefficient, $\tilde{D}_{Cr,Mn}$. The interdiffusion coefficient was found to be independent of composition in the temperature range investigated. The samples exhibited no Kirkendall porosity, indicative of a complete homogeneous solid solution. The calculated values of $\tilde{D}_{Cr,Mn}$ are plotted as a function of temperature in fig. 3b. The chromium and manganese exchange sites via cation interstitials and the interdiffusion coefficient is given by:

$$\tilde{D}_{Cr,Mn} = 0.361 \exp(-378.3\ \mathrm{KJ/RT})\ \mathrm{cm^2\ s^{-1}}. \quad (3)$$

The extent of the interdiffusion was estimated using the above equation and the following method. Assuming a limit of 50% Cr site exchange for Mn as the criterion for cell failure, the error function approach using $\mathrm{erf}(0.5) = 0.5$ provides a mathematically convenient marker with the relation:

$$x = (\tilde{D}t)^{1/2}. \quad (4)$$

The results using the above equation are tabulated for various temperatures of interest in table 1. The interdiffusion described above is quite general in the case of perovskites. The extent of interdiffusion is

Table 1
Cr–Mn interdiffusion distance as a function of time and temperature.

Time		Distance (cm)			
(months)	(s)	$X_{800°C}$	$X_{900°C}$	$X_{1000°C}$	$X_{1100°C}$
1	2.63×10^{6}	6.09×10^{-7}	3.74×10^{-6}	1.70×10^{-5}	6.24×10^{-5}
6	1.58×10^{7}	1.49×10^{-6}	9.15×10^{-6}	4.16×10^{-5}	1.53×10^{-4}
12	3.15×10^{7}	2.11×10^{-6}	1.29×10^{-5}	5.88×10^{-5}	2.16×10^{-4}
18	4.73×10^{7}	2.59×10^{-6}	1.59×10^{-5}	7.20×10^{-5}	2.65×10^{-4}
24	6.31×10^{7}	2.99×10^{-6}	1.83×10^{-5}	8.32×10^{-5}	3.05×10^{-4}

strongly influenced by the choice of processing temperatures and materials in question. Since the diffusion process is thermally activated, lower processing and operating temperatures are recommended. For thin-film devices in particular, the performance obtained is critically dependent on the processing and device operating conditions.

3.2. Interdiffusion at perovskite electrode/electrolyte interfaces

In the La(Sr)MnO_3–YSZ system formation of interface reaction products were observed when the cathode/electrolyte couple were exposed to temperatures in excess of 1300°C. As seen in fig. 4a, diffusion of manganese into the electrolyte occurs predominantly along the grain boundaries. The effects of this are to create electronic shorts which lead to a lowering of the faradaic efficiency of the cell. Another consequence of high-temperature interactions between perovskite electrodes and zirconia electrolytes is formation of the $La_2Zr_2O_7$ phase at the cathode interface. This was identified using a La(Sr)MnO_3–YSZ diffusion couple and analyzed

(a)

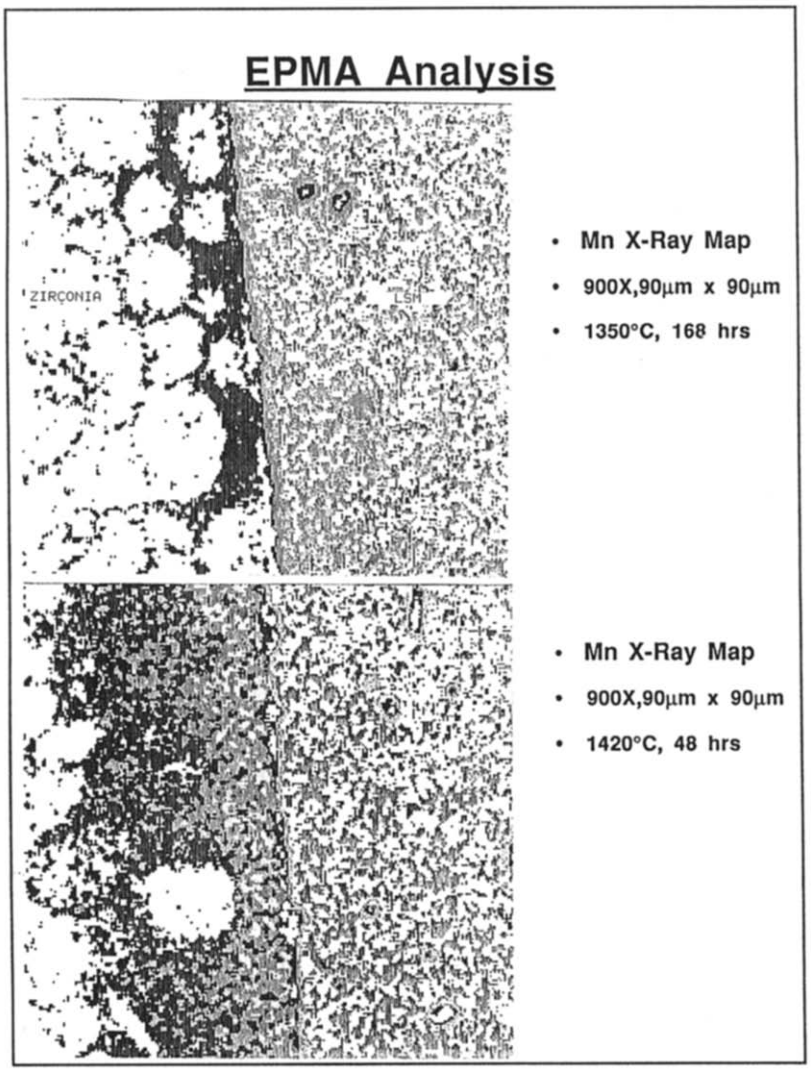

Fig. 4. (a) Mn interdiffusion at the cathode (LSM)–electrolyte (YSZ) interface.

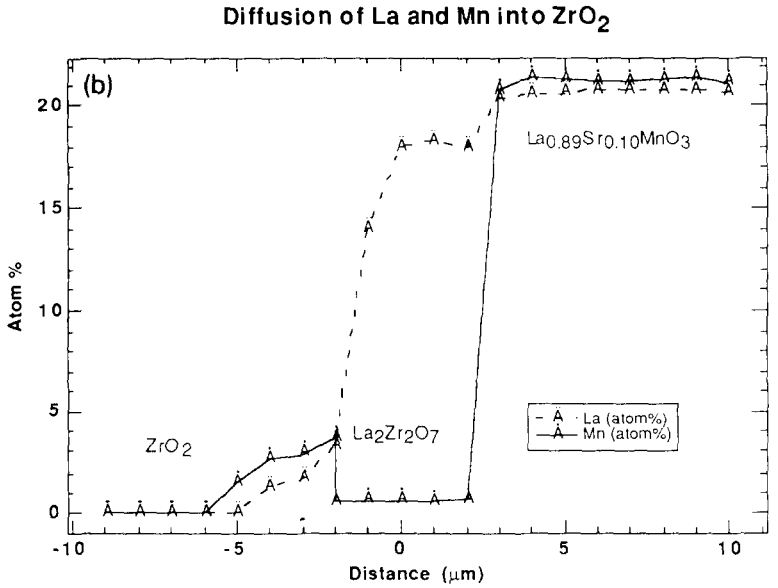

Fig. 4. (b).

using electron-probe microanalysis as shown in fig. 4b. This pyrochlore phase has a conductivity about 3–4 orders of magnitude lower than that of the electrode materials and thus is manifested as an increase in the "interface" resistance. The stability of such perovskites against reactions with zirconia-based electrolytes has been studied [11], and is generally dependent on the B-site cation. As device temperatures are lowered, the perovskite electrode material often chosen is doped $LaCoO_3$ based on the conductivity of the material. This material, however, also exhibits greater reactivity with the electrolyte.

Fig. 5 shows the impedance of cathode half cells fabricated under controlled electrode firing condi-

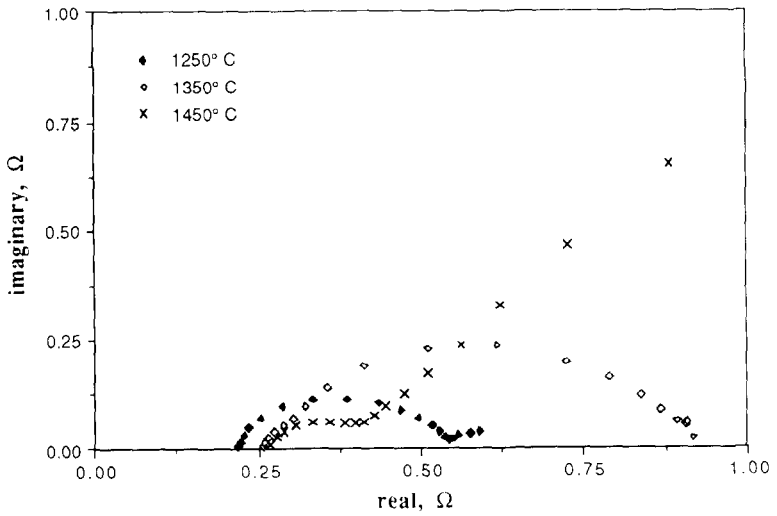

Fig. 5. Impedance behavior of cathode half cells with cathodes fired at 1250, 1350 and 1450°C.

tions. For cells fabricated with electrodes fired at temperatures greater than 1350°C, an additional arc is observed at lower frequencies in the impedance spectrum. The electrode arcs have typical relaxation frequencies of about 1 kHz and about 55 Hz. This latter arc is attributed to the presence of interface reaction product phases. Our studies on ZrO_2/LSM diffusion couples at 1450°C clearly show the formation $La_2Zr_2O_7$ phase, about 10 μm thick, at the interface. When reacted in powder form the ZrO_2/LSM mixture forms the pyrochlore phase even at 1300°C [2]. In addition, extensive diffusion of manganese along the grain boundaries was also observed. Reactivity studies [1] between LSM and ZrO_2 identified a quaternary $ZrO_2.Y_2O_3.MnO_x.LaO_y$ along with the pyrochlore phase, when reacted at 1000°C for 1728 h. Since the experimental design employed lends itself to isolating one electrode–electrolyte interface, the analysis of the LSM/ZrO_2 interface becomes rather straightforward. An electrical analog of this phenomenon has been modeled to simulate the impedance spectra. The analog takes into account the change in interfacial characteristics due to formation of a second phase as well as diffusion of manganese from the cathode.

3.3. Effect of thermal cycling on cell performance

Using the appropriate reference electrodes and counter/working electrodes, impedance data were obtained for the cell including the electrodes, the electrolyte and the platinum current collector grid and the anode and cathode interfaces separately. The EIS spectra were characterized by one semicircular arc for the total cell and the cathode with the anode exhibiting two distinct arcs. The high-frequency intercept of the locus of the impedance arcs on the real axis, given by R_∞ is attributed to the bulk ohmic resistance including the current collector–electrode contact resistance, while R_1 and R_2, etc. are related to the electrodes. Correspondingly in fig. 6a, R_∞ is principally attributed to the resistance of the gap between the working and reference electrodes, while R_1 and R_2 are associated with the electrode processes. The data indicate that the cell impedance spectra expand with thermal cycle number, indicating a consistent increase in the cell impedance. The change of R_∞, for the cell and each electrode, with thermal cycle are plotted in fig. 6b.

The data indicate that the R_∞ values for the cell increase as do the $R_{(\infty,\text{anode})}$, with the cathode remaining constant. A similar analysis for the electrode processes show that ($R_{1(\text{cathode})}$), corresponding to the oxygen reduction process at the cathode, increases monotonically with thermal cycle. On the anode, however, the relative variation of the $R_{1(\text{anode})}$ and $R_{2(\text{anode})}$ increases dramatically with a brief interruption in the fuel gas manifold composition from H_2–3%H_2O to air. These changes can be understood by considering that the nickel in the two-phase Ni–ZrO_2 anode cermet undergoes rapid oxidation upon contact with air at 1273 K. Upon re-heating the anode under H_2–3%H_2O as fuel gas, the anode is reduced again. This phase change, however, results in a decrease in contact area due to the volume expansion and contraction in contact with air and H_2 respectively. The effect of increasing R_1 with thermal cycle is attributed to change in the contact area between nickel and ZrO_2 substrate due to the difference in thermal expansion coefficients between the two phases. This results in an increase of the migration paths of oxygen ions before they are oxidized at the Ni–ZrO_2 interface.

A model describing the kinetics of nickel grain growth on the surface of ZrO_2, thus resulting in increasing the interfacial impedance of the electrodes, is used to describe the changes in EIS spectra [12]. This model can quantitatively estimate the rate of nickel coarsening based on bulk diffusion of nickel and correlate that with the change in electrode polarization with time and temperature. While the effect is on electrode polarization, the origin is in the non-wetting behavior of nickel, and is thus included as a "materials"-related degradation. Such degradation is inevitable in non-wetting metal–ceramic systems and the only possibility to achieve stable operation is to either slow the kinetics of nickel growth via lower-temperature operation or choosing an electrode-electrolyte system which allows compatible wetting behavior to be obtained.

4.4. Lumped parameter cell circuit model

From the above results and discussions, it is apparent that materials and their interactions often play a dominant part in determination of the performance of high-temperature cells. The impedances as-

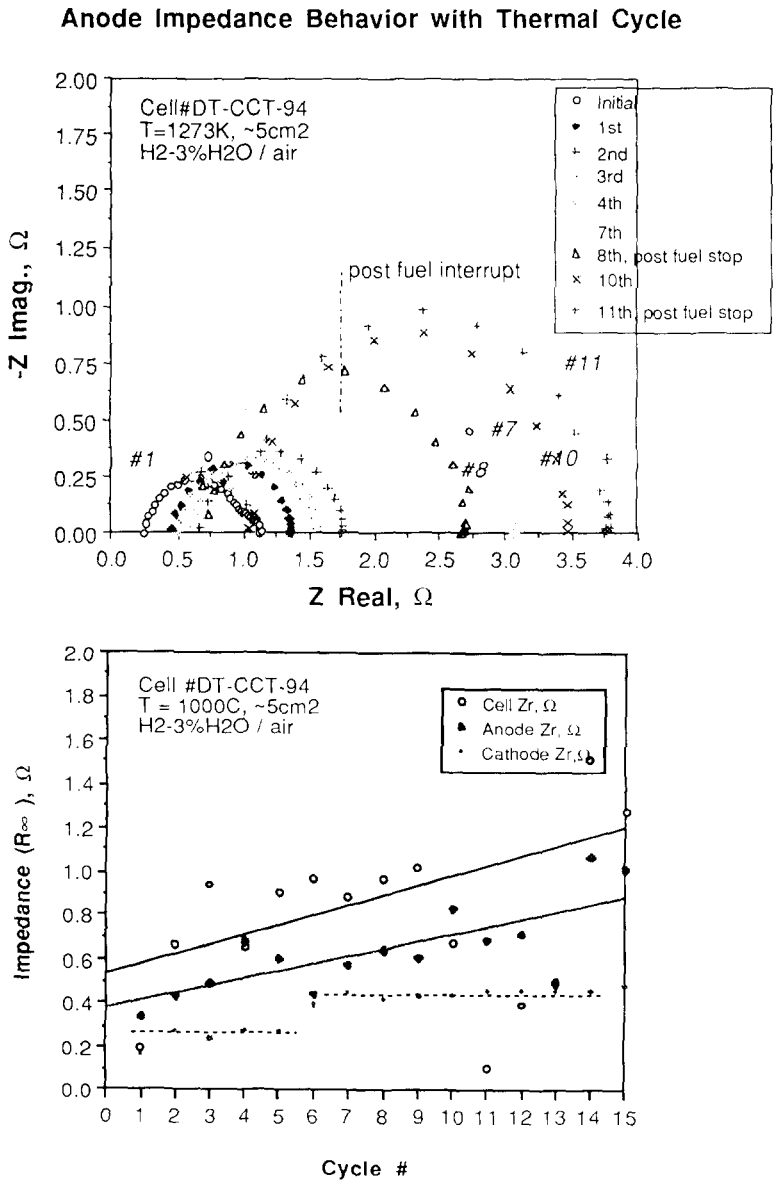

Fig. 6. Thermal cycle related cell performance degradation.

sociated with the different materials and interfaces can be evaluated using the EIS technique with proper cell design. A typical circuit for an SOFC cell can be constructed using five circuit elements as shown in fig. 7. While such a cell representation can be made to adequately fit typical impedance spectra as shown in fig. 6a, separation of the individual interfaces is not possible. In order to determine the various ma-

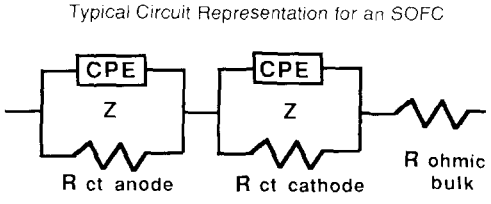

Fig. 7. Typical circuit representation for an SOFC.

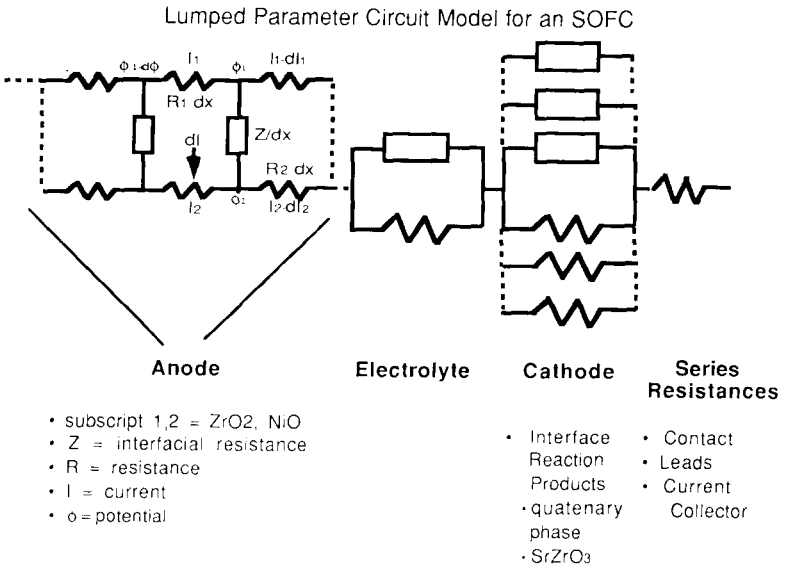

Fig. 8. Lumped parameter circuit model for an SOFC.

terials' contributions, a more detailed circuit model can be constructed as shown in fig. 8. This model can account for the changes in cell performance by measurement and analysis of the cell impedance response. The circuit elements can be collected together into three groups: a lumped series resistance consisting of ohmic contributions of the electrolytes and electrodes, interface reaction products, and current collector contact resistances; parallel resistances related to formation of electronic shorts through the electrolyte structure; and a transmission line behavior impedance associated with metal–ceramic composite electrodes.

The contribution of each of these lumped impedance parameters to the overall cell impedance depends on various factors such as the materials of cell construction, operation temperature, effect of time and thermal cycling. While an a priori deconvolution of the impedance spectrum is rather complex, the various studies carried out as in the present case permit the interpretation of the observed cell behavior based on the dependences of the performance on the temperature and other cell conditions. Based on extensive investigations in the authors' laboratories, the following general effects can be expected:

4.4.1. Effects of time

This has perhaps the most significant effect on cell performance especially if one or both of the electrodes have non-wetting characteristics. Due to metal coarsening behavior, this impedance increases with time.

For reactive electrodes, the development of a resistive film at the interface with the electrolyte also causes an increase in the series resistance. In addition, an additional impedance due to slow mass transport kinetics can be observed and distinguished from the formation of resistive layers by a usually lower (few Hz) characteristic frequency and partial pressure dependence.

4.4.2. Effects of thermal cycling

Especially for electrodes with poor match in thermal expansion coefficients, an increase in both the series resistance and electrode reaction impedance may be observed. The latter can be distinguished by a characteristic dependence on partial pressures, depending on the reaction mechanism.

4.4.3. Effect of temperature

For cells fabricated and operated within the thermodynamic stability limits of the materials, no impedances due to interfacial degradation are nec-

essarily observed. However if stability limits are exceeded then either series resistances and/or parallel impedances due to diffusion reactions may appear.

5. Summary and conclusions

A review of materials investigations and a detailed lumped parameter circuit model for a typical high-temperature solid oxide fuel cell is determined. Materials contributions and their relation to interfacial impedances have been studied. Experimental techniques to contrast this materials irreversibility from electrode kinetic reversibility are outlined. Conventional techniques for microanalysis of the solid–solid interfaces of high-temperature cells when coupled with transient dc and EIS techniques can be useful in distinguishing between the formation of resistive interfacial layers, poor electrode contact and electrode densification. Finally, on the basis of these investigations, a lumped parameter circuit model of a typical high-temperature cell is derived. The circuit elements describe the various physical and mechanistic processes occurring at the electrodes and their interfaces. Careful analysis of the cell performance in relation to such a circuit model allows one to examine degradation causes and potentially determine ways of increasing cell stability. For stable and high performance of high-temperature cells, a detailed study of causal relationships between cell materials, processing conditions and cell performance is necessary.

Acknowledgements

This work was supported by the Gas Research Institute, Basic Science Division, under Contract No:5086-294-1292. The authors would also like to thank for many discussions with Prof. A. Virkar, C. Milliken and M. Timper.

References

[1] S.K. Lau and S.C. Singhal, Corrosion 85 (NACE, March 1985) Abstract No. 345.
[2] O. Yamamoto, Y. Takeda, R. Kanno and T. Kojima, Proc. SOFC, Nagoya, Japan, 1989.
[3] A.C. Khandkar, S. Elangovan, M. Liu and M. Timper, Proc. Symp. on High-Temperature Electrode Materials and Characterization, Vol. 91-6, eds. D.D. Macdonald and A.C. Khandkar (Electrochem. Soc., Pennington, NJ, 1991) p. 175.
[4] S. Elangovan, A.C. Khandkar, M. Liu and M. Timper, Proc. Symp. on High-Temperature Electrode Materials and Characterization, Vol. 91-6, eds. D.D. Macdonald and A.C. Khandkar (Electrochemical Society, Pennington, NJ, 1991) p. 191.
[5] C. Milliken, D. Tucker, S. Elangovan and A. Khandkar, 1990 Fuel Cell Seminar (Phoenix, AZ, 1990).
[6] C. Milliken, D. Tucker, S. Elangovan and A. Khandkar, Ext. Abstracts, 177th ECS Meeting (Montreal, Canada, 1990).
[7] M.C.H. McKubre, S.I. Smedley and F.L. Tanzella, Proc. Symp. on High-Temperature Electrode Materials and Characterization, Vol. 91-6, eds. D.D. Macdonald and A.C. Khandkar (Electrochem. Soc., Pennington, NJ, 1991) p. 207.
[8] M. Liu and A.C. Khandkar, Extended Abstracts of the Electrochem. Soc. Meeting, 90-2 (Seattle, WA, 1990) Abstract No. 746.
[9] R. Koc, H.U. Anderson and S.A. Howard, Proc. 1st Intern. Symp. on Solid Oxide Fuel Cells, Vol. 89-11 (Electrochem. Soc., Pennington, NJ, 1989) p. 220.
[10] C. Matano, Japan J. Phys. 8 (1984) 109.
[11] Yokokawa, Proc. SOFC (Nagoya, Japan, 1989).
[12] S. Elangovan and A. Khandkar, Proc. 1st Intern. Symp. on Ionic and Mixed Conducting Ceramics, Vol. 91-12, eds. T.A. Ramanarayanan and H.L. Tuller (Electrochem. Soc., Pennington, NJ, 1991).